Available online at www.sciencedirect.com
ScienceDirect
International Journal of Mechanical Sciences 48 (2006) 1264–1272
International Journal of MECHANICAL SCIENCES
www.elsevier.com/locate/ijmecsci

A new upper bound solution for analysis of the radial forging process

A. Ghaei[a], A. Karimi Taheri[b,*], M.R. Movahhedy[a]

[a]Department of Mechanical Engineering, Sharif University of Technology, Tehran, Iran
[b]Department of Materials Science and Engineering, Sharif University of Technology, Tehran, Iran

Received 5 August 2004; received in revised form 13 May 2006; accepted 4 June 2006
Available online 2 August 2006

Abstract

Radial forging is an open die forging process used for reducing diameter of shafts, tubes, stepped shafts and axels, and creating the internal profiles for tubes such as rifling the gun barrels. In the present research, a new model based on calculating the deformation work was developed to find an upper bound limit for the deformation load in the case of radial forging of rods and tubes. Also, the model was used to assess the effects of the process parameters. The accuracy of the model was tested by comparing the predicted results with those achieved from the experiment at work of Uhlig [Investigation of the motions and the forces in radial swaging. Doctoral Dissertation, Technical University Hannover, 1964]. A good agreement was found between the two sets of results.

Keywords: Radial forging; Upper bound method; Deformation analysis

1. Introduction

Radial forging is a hot or cold forging process utilizing two or more radially moving anvils, or hammer dies, to produce solid or tubular components with constant varying cross sections along their length. This process is usually used to reduce the diameters of ingots and bars, forging of stepped shafts and axels, forging of guns and rifle barrels, and production of tubular components with or without internal profiles [2].

Deformation in radial forging results from a large number of short-stroke side-pressing operations performed usually by four forging tools arranged radially around the workpiece. A typical hammer-type arrangement is shown schematically in Fig. 1. The forging action of the radial forge takes place within a vertically arranged forging box housing the four hammers and two drives located at right angles to one another. Due to opposing motion of the hammers, no force is transmitted to the machine base [3].

Tszeng and Kobayashi [4] were the first to model the process of tube forging using the FEM. Domblesky et al. [5] presented a finite element model to determine the strain, strain rate, and temperature distribution in radial forging. Jang and Liou [6] also modeled radial forging by the finite element method (FEM) to evaluate the residual stresses. Using the slab method of analysis, Lahoti et al. [7,8] analyzed the mechanics of radial forging process for both the single and compound angle dies. Employing a modular upper bound technique, Subramanian et al. [9] modeled the metal flow in die cavity in radial forging for rifling of the gun barrels under plane strain condition. The aims of their study were both to investigate the metal flow in rifling of gun barrels and to determine the influence of process variables on metal flow. So, their model was limited to modeling of the material flow in rifling of the gun barrels and thus was not capable of modeling the deformation pattern in the process of radial forging. On the other hand, they didn't consider all of the three zones of deformation existing in the radial forging process including the sinking, forging and sizing zones. They also used physical modeling by conducting large-scale strain compression tests using a die cavity shaped in the form of rifling in a small caliber gun barrel. Yang [10] conducted a study on the radial forging process using the combination of slip-line theory with the upper bound method under plane strain condition. He used the slip line field and a hodograph coupled with

*Corresponding author.
E-mail addresses: ghaei@mehr.sharif.edu (A. Ghaei), ktaheri@sharif.edu (A. Karimi Taheri), movahhed@sharif.edu (M.R. Movahhedy).

0020-7403/$ - see front matter © 2006 Elsevier Ltd. All rights reserved.
doi:10.1016/j.ijmecsci.2006.06.002

Nomenclature

A	cross-sectional area of the element at the end of step
A_s	cross-sectional area of the element at the start of step
A_{fric}	contact area at die–part interface
A_{s1}, A_{s2}	shear surfaces (Fig. 6)
e	length of deformation step in the radial direction (Figs. 4(a) and (b))
F_r	radial force applied to hammer dies
F_{siz}	force due to the deformed material in the sizing zone that applies to the dies
k	yield shear stress of the part
L_1	length of the sinking zone
L_2	length of the forging zone
L_3	length of the sizing zone
m	friction shear factor
R	outer radius of the element
R_m	radius of the mandrel
R_0	outer radius of the preform
R_1	inner radius of the preform
R_2	outer radius of the product
R_s	outer radius of the element at the start of deformation step
t	thickness of the element at the end of step
t_s	thickness of the element at the start of step
t_0	thickness of the preform
V	the element volume
W_{f1}	friction work at the part–die interface in the sinking zone
W_{fm2}	friction work at the part–mandrel interface in the forging zone
W_{fm3}	friction work at the part–mandrel interface in the sizing zone
W_{fd2}	friction work at the part–die interface in the forging zone
W_{fd3}	friction work at the part–die interface in the sizing zone
W_{s1}, W_{s2}	shear work over the surfaces A_{s1}, A_{s2}
W_{s3}	shear work over the surface adding material to the sinking zone
W_{p1}, W_{p2}	plastic work at the sinking and forging zones, respectively
Δs	amount of element movement in the direction of material flow (Figs. 4 and 5)
α	die angle
ε_r	strain in the radial direction
ε_θ	strain in the circumferential direction
ε_z	strain in the axial direction
$\bar{\varepsilon}$	effective strain
$\bar{\sigma}$	flow stress of the material in compression

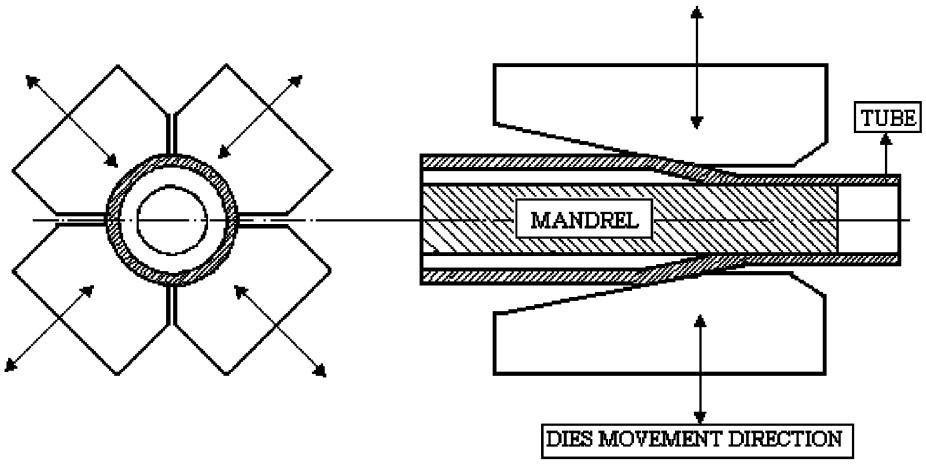

Fig. 1. Typical tool arrangement in radial forging.

the use of a non-linear optimization technique to find the field angles and other defining parameters. The results of his study showed that this procedure provides a powerful method for calculating the complicated slip-line field solutions. Thompson et al. [11] presented a steady-state approximation technique for the analysis of radial forging. Their approximation was used with the finite element method to determine the billet temperature and deformation during the forging process.

During the manufacture of tubular products employing radial forging, the forging pressure, the state of stress and also the flow pattern are influenced by various parameters such as reduction in cross-section area, the shape of both the hammer dies and the mandrel, the frictional conditions

at the interfaces and the flow properties of the material. Interactions of some of these parameters with each others often make it difficult to find an exact mathematical solution to predict the real phenomenon occurring in the process. For this reason, approximate methods both analytical and numerical have been developed.

Up to now, the radial forging process has been modeled by both the slab and the finite element methods. Although, simulations based on the FEM method are capable of predicting many variables in the process such as strain, strain rate and stress distributions somewhat more accurately, but to obtain these are often very time consuming and computationally more expensive. Therefore, simplified methods such as the upper bound method when applied properly can yield the answers rapidly while being very effective. To our knowledge, a detailed and complete analysis of the radial forging process itself, based on the upper bound analysis has not been presented in the literature. Thus, the purpose of the study was to estimate the load applied on the die during the radial forging process using a new upper bound solution.

In general, an upper bound technique is based on calculating the required power in the process using a kinematically admissible velocity field, but in this study a direct work-based analysis is presented in order to determine the load applied to the hammers during the radial forging process itself [12–17].

2. Analysis

The general model of the radial forging process for tubes, considered in this study, is shown schematically in Fig. 2. It is assumed that there is no material spreading between the hammer dies at the end of the blow, thus, ensuring a two-dimensional material flow. Again, the effect of material spreading on the plastic work is neglected, however, the effect of clearance between the hammer dies on the friction work at the end of the blow is considered. In general there is a small gap between the mandrel and the inner surface of the billet. In other words, forging under the conical portion of the hammer dies is accompanied by a certain amount of sinking. This sinking causes a longitudinal back-push applied on the billet at the radial plane where the inner surface of the tube first touches the mandrel. In addition, the hammer dies also contain a cylindrical sizing zone. Nearly all the deformation occurs in the conical inlet section, i.e., in the forging zone (II) shown in Fig. 2. In the sizing zone (III), most of the tube material is elastically deformed to the yield limit and only a small amount of plastic deformation takes place. Nevertheless, a considerable amount of energy, supplied by the dies, is needed for this operation. Thus, as shown in Fig. 2 there are three distinct regions of deformation in radial forging of the tubes: (a) the sinking zone (I); (b) the forging zone (II); and (c) the sizing zone (III). In the following analysis of the process, all three zones are considered. It is obvious that in some cases, such as during finish forging of the tubes, the sinking zone may be very small and its contribution to the overall radial forging load may then be excluded in the final evaluation of the estimates to the loads [7].

Depending on the inlet cone angle of the hammer die, α in Fig. 3, and the friction at the tube–die and the tube–mandrel interfaces, along with axial push and pull forces, and also length of the die land, the deforming material may flow relatively either towards the product or towards the preform or in both of these directions simultaneously. Thus, in an almost general case, a neutral plane may exist somewhere, within the deforming tube, as indicated schematically (N–N) in the section marked II in Fig. 2. The material being exactly on this neutral plane (N–N), is only deformed radially and does not flow axially. On both sides of the neutral plane (N–N), the metal is deformed both radially as well as axially, thus it flows away from the neutral plane (N–N) in both directions, i.e. either towards the preform or the product. Theoretically, the neutral plane (N–N), could lie in one of the three zones of deformation. However, it is usually located in the forging zone in most of the practical conditions, see Ref. [7]. Therefore, it may be an acceptable engineering accuracy to assume that the neutral plane (N–N), lies in the middle of the forging zone. The axial feed makes a secondary forging zone being practically a small zone relative to the other zones and its contribution to the total work can therefore be neglected.

The total work required for the process is divided into three components; (a) the plastic work or strain energy, (b)

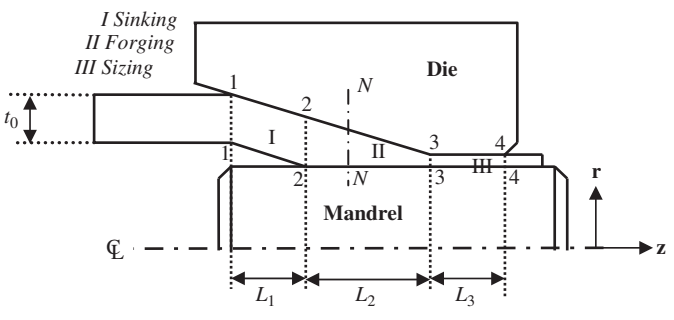

Fig. 2. Schematic representation of the radial-forging process for tubes.

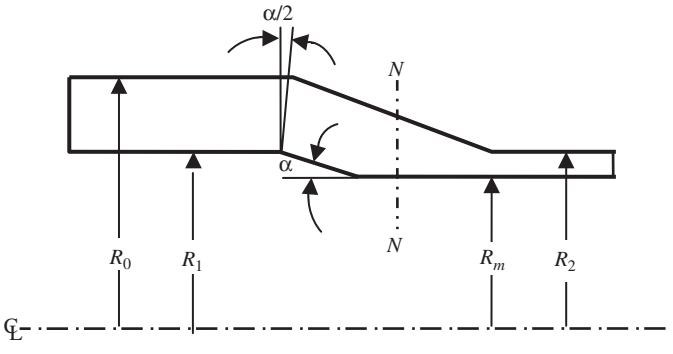

Fig. 3. Schematic representation of radial forging for tubes and variables.

the frictional work, and (c) the shear work which is dissipated when the material flow direction is changed. The stroke is divided into many small displacements and it is assumed that the stress and strain is constant throughout each element in each step and the work is calculated in the last step of the stroke.

In the present analysis, the total work required for the process is obtained using the following assumptions:

1. The material is rigid-plastic.
2. Friction at the die-tube and at the mandrel–tube interfaces produces a constant frictional shear stress $\tau = mk$ at these surfaces, where, $0 \leqslant m \leqslant 1$ and k is the yield shear stress.
3. The wall thickness of the tube remains constant throughout the sinking zone.
4. The stress and strain are homogenous in each element.
5. There are no front-pull and back-push forces.
6. The neutral plane (N–N), is at the middle of the forging zone. So, the material initially existing between the preform and this plane flows towards the preform, and the material existing between the part and this plane flows towards the product.

2.1. Analysis from the middle of the forging zone (N–N), to the sinking zone (I)

2.1.1. Forging zone

As the radial forging dies strike, the outer radius is reduced and the material flows axially. The element being exactly located in the neutral plane (N–N) is thus deformed only radially. So, this element elongates, as $\varepsilon_z\,\mathrm{d}z$ in the axial direction. To the left, this element then pushes the neighboring element towards the preform, while the neighboring element elongates itself too. Thus, the total amount of movement in the axial direction for each elemental step is equal to its axial elongation plus the movement of the previous element viz.

$$\Delta s_{\text{step}} = \Delta s_{\text{previous element}} + \varepsilon_z\,\mathrm{d}z. \tag{1}$$

Since the location of each element is known at the start of each deformation step, and as the amount of axial movement of the element can be obtained by Eq. (1), therefore, the radius of the final location of the element is given by Eq. (2) (see Fig. 4(a) for movement towards the left of neutral plane (N–N)).

$$R = R_s - e + \Delta s \times \tan\,\alpha. \tag{2}$$

The thickness of the each element at the start and end of deformation step is given by

$$t_s = R_s - R_m, \tag{3}$$

$$t = R - R_m. \tag{4}$$

Now since, the location of the element is defined, the strains can be calculated. The radial, average circumferential and axial strains are respectively given by;

$$\varepsilon_r = \ln\left(\frac{t}{t_s}\right), \tag{5}$$

$$\varepsilon_\theta = \ln\left(\frac{R - t/2}{R_s - t_s/2}\right), \tag{6}$$

$$\varepsilon_z = -(\varepsilon_r + \varepsilon_\theta) \tag{7}$$

while the effective strain is

$$\bar{\varepsilon} = \sqrt{\frac{2}{3}(\varepsilon_r^2 + \varepsilon_\theta^2 + \varepsilon_z^2)}. \tag{8}$$

The element volume is given by

$$\mathrm{d}V = \pi(R^2 - (R - R_m)^2)\,\mathrm{d}z. \tag{9}$$

The plastic and frictional work for each element at the tube–mandrel and at the tube–die interfaces are obtained by

$$W_{p2} = \bar{\sigma}\,\bar{\varepsilon}\,\mathrm{d}V, \tag{10}$$

$$W_{fm2} = (m\,k)(2\pi R_m\,\mathrm{d}z)(\Delta s), \tag{11}$$

$$W_{fd2} = (m\,k)(A_{fric})\left(\frac{\Delta s}{\cos\,\alpha}\right). \tag{12}$$

2.1.2. Sinking zone

Since, it was assumed that thickness of the tube remains constant in this zone, the material flows along the die surface, see Fig. 5. As the hammer dies strike, both the outer and the inner radii of the elements are reduced. Therefore, the amount of movement of the first element is equal to movement of the latest element in the forging zone divided by $\cos\alpha$. The amount of movement of other elements can then be determined by

$$\Delta s_e = \Delta s_{\text{previous element}} + \frac{\varepsilon_z\,\mathrm{d}z}{\cos\,\alpha}. \tag{13}$$

Radius of the element in the final location R, similar to that shown in Fig. 4(b), is given by

$$R = (R_s - e) + \Delta s \times \sin\,\alpha. \tag{14}$$

The cross-sectional area of the element at the start and at the end of each step is, respectively calculated by

$$A_s = \pi\,t_0(2R_s - t_0\,\cos\,\alpha), \tag{15}$$

$$A = \pi\,t_0(2R - t_0\,\cos\,\alpha). \tag{16}$$

As the variation in wall thickness of the tube in the sinking zone is disregarded, the radial strain is zero. Therefore, the incremental strain in the z-direction is equal to the variation in cross-sectional area of the element:

$$\mathrm{d}\varepsilon_z = -\frac{\mathrm{d}A}{A} \rightarrow \varepsilon_z = \ln\left(\frac{A}{A_s}\right). \tag{17}$$

The effective strain is given by

$$\bar{\varepsilon} = \frac{2}{\sqrt{3}}\varepsilon_z. \tag{18}$$

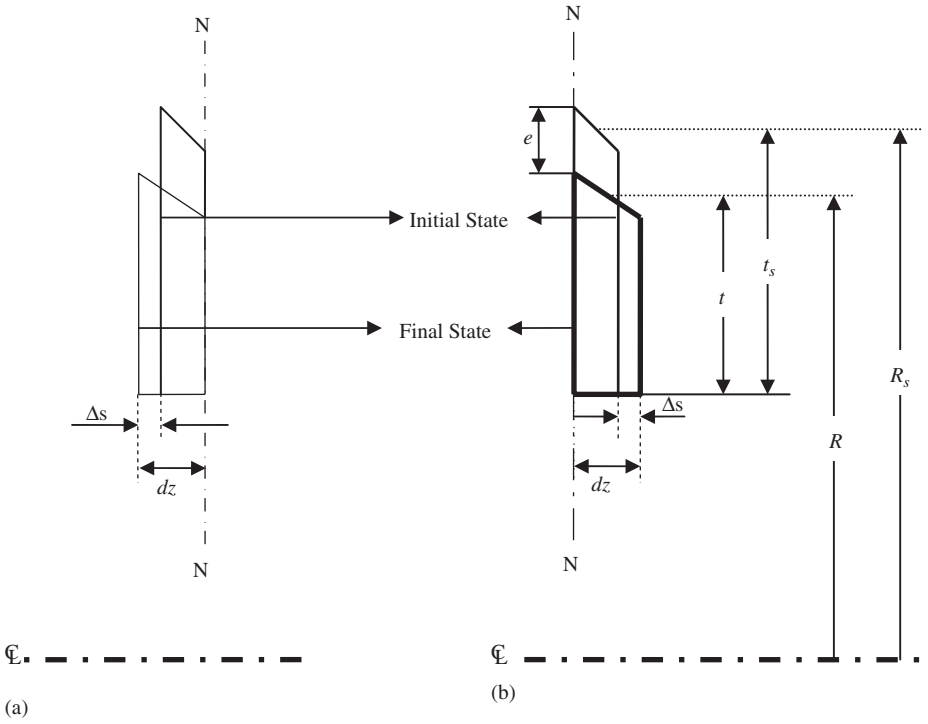

Fig. 4. The element located in forging zone.

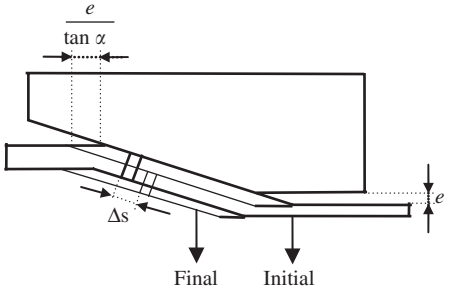

Fig. 5. The element located in sinking zone.

The plastic and frictional works for each element can be determined respectively as

$$W_{p1} = \bar{\sigma}\,\bar{\varepsilon}\,\mathrm{d}V, \tag{19}$$

$$W_{f1} = (m\,k)\left(A_{fric}\frac{\mathrm{d}z}{\cos\alpha}\right)(\Delta s). \tag{20}$$

2.2. Analysis from the middle of the forging zone to the sizing zone (III)

2.2.1. Forging zone

Following a similar approach to that presented in Section 2.1.1, the amount of movement for each element in the forging zone (II), is determined using Eq. (1). Again, the initial location of the element is known and the radius of element at the final location, see Fig. 4(b), is evaluated by

$$R = (R_s - e) - \Delta s \tan\alpha. \tag{21}$$

Since, both the radii at the initial and the final positions are known; the strains can be determined using Eqs. (3)–(8). Similarly, the plastic and frictional works are determined using Eqs. (10)–(12).

2.2.2. Sizing zone

Neglecting the small portion of plastic deformation in the sizing zone, the amount of movement in this zone is equal to the movement of the last element in the forging zone. The frictional works between the mandrel–tube and the die–tube interfaces are respectively determined by

$$W_{fm3} = (m\,k)(2\pi\,R_m\,L_3)\left(\Delta s + \frac{e}{\sin\alpha} - \frac{e}{\tan\alpha}\right), \tag{22}$$

$$W_{fd3} = (m\,k)(A_{fric})\left(\Delta s + \frac{e}{\sin\alpha} - \frac{e}{\tan\alpha}\right), \tag{23}$$

where, Δs as before is obtained from the forging zone.

Again, as mentioned earlier, the material exiting the sizing zone is deformed and a considerable amount of energy is required for this operation. The results of FEM simulations of the process conducted by Ameli [18] also show that stress in the sizing zone reaches to the yield stress according to the Von-Mises yield criterion. Therefore, the contribution of this energy to the overall radial load is of some importance. As the axial stress (the largest stress) is

positive and the radial stress (the smallest stress) is negative, the flow stress is larger than the radial pressure. Thus, the maximum radial load required to perform such a deformation may be written as

$$F_{siz} = 2\pi R_2 L_3 \bar{\sigma}. \tag{24}$$

2.3. Shear work

Considering the flow pattern depicted in Fig. 6, the material changes its flow directions both at the start and at the end of the sinking zone. As shown in Fig. 6, at the end point the material flows backwards and changes its direction by shear. However, mechanics of the deformation at the start point of the sinking zone is rather complicated, because some material is flowing backwards while, some is added to the sinking zone due to the axial feed of the preform. The interaction of these two motions is thus not exactly clear. Moreover, the tube is certainly bent and this makes it difficult to calculate the plastic work expenditure exactly. Neglecting this interaction, shearing occurs while the dies are striking. As shown schematically in Fig. 6, the material is flowing backwards and sheared over marked surfaces A_{s1} and A_{s2}. The amount of material passing through these surfaces is determined by Eqs. (1) and (13), respectively. Therefore, each shear work is given by

$$W_{s1} = k \tan(\alpha) A_{s1} \Delta s, \tag{25}$$

$$W_{s2} = k \tan(\alpha/2) A_{s2} \Delta s \cos(\alpha/2), \tag{26}$$

where

$$A_{s1} = \frac{\pi t_0}{\cos \alpha}\left(2R_m + \frac{t_0}{\cos \alpha}\right) \tag{27}$$

and

$$A_{s2} = \frac{\pi t_0}{\cos(\alpha/2)}(2R_0 - t_0). \tag{28}$$

The third shear work due to adding of the material into the sinking zone (hatched portion shown in Fig. 7) is given by

$$W_{s3} = k \tan(\alpha/2)\pi[R_0^2 - (R_0 - t_0)^2]\frac{e}{\tan \alpha}. \tag{29}$$

The total work is obtained by adding all of the works calculated above. The radial load (F_r) applied to the dies is obtained by dividing the total work by the stroke step.

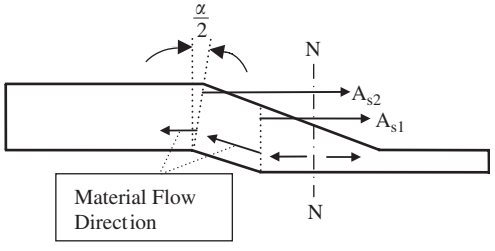

Fig. 6. Material flow direction and shear surfaces.

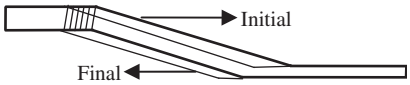

Fig. 7. Schematic representation of adding material from preform to the sinking zone.

Thus,

$$W_{total} = (W_{p1} + W_{p2}) + (W_{f1} + W_{fm2} + W_{fd2} + W_{fm3} + W_{fd3}) + (W_{s1} + W_{s2} + W_{s3}), \tag{30}$$

$$F_r = \frac{W_{total}}{e} + F_{siz}, \tag{31}$$

where F_{siz} is the radial load applied by sizing zone which was given earlier in Eq. (24).

3. Results and discussion

In order to calculate the total radial forging load, the dimensions of the three zones of deformation were calculated from both the tool and workpiece geometry. Each of the three zones was divided into several ring-shaped elements. The press stroke was divided into very small displacements so that the strain and frictional works can be assumed to be constant at each deformation step.

As the experimental results on loads were not available for the radial forging of tubes in the present research, the loads measured earlier by Uhlig [1] for cold swaging of AISI 1015 steel rounds and those also used by Lahoti and Altan [7], were used to verify the loads predicted by the present analysis. Again, as the measured data given in Ref. [1] was based on cold work, where the work hardening induces a considerable effect on the flow stress data, an equivalent stress–strain relationship of the type $\bar{\sigma} = K\bar{\varepsilon}^n$ was assumed for the billet material. Both the factor K and n value at the room temperature were assumed to be as given by Altan et al. [2]:

$$K = 618.14 \text{ MPa}, \quad n = 0.1184.$$

Again, since in the present analysis, the material was assumed to be rigid-plastic, an average flow stress $\bar{\sigma}$, for both the preform and the part was used. According to above analysis, the amount of each work was calculated for the final deformation step. The followed approach was based on predicting a maximum load during the process. Employing the analysis, the predicted loads for the various samples (1)–(4) with the initial billet diameter varying as 15.97–13.99 mm, are given in Table 1, where these results are compared with both the experimental data measured by Uhlig [1] and the predicted results by Lahoti and Altan using the slab method analysis in Ref. [7].

According to the results shown in Table 1, the predicted loads show a reasonably fair to good agreement with experiments. It is interesting to note that the results of slab method [7] show a good agreement for samples (1) and (2),

Table 1
Comparison of predicted loads with experimental results [1]

Sample number	Billet diameter (mm)	Product diameter (mm)	Length of forging zone (mm)	Length of sizing zone (mm)	Predicted load[a] by slab (*KN*) Ref. [7]	Predicted maximum load[a] (*KN*)	Load[a] from experiment (*KN*) Ref. [1]
1	15.97	13.18	18.55	18.00	171.98	193.22	172.00
2	15.97	13.25	18.09	18.00	170.62	190.42	167.00
3	15.03	13.11	12.77	18.00	143.37	149.79	124.00
4	13.99	13.03	6.38	18.00	106.18	105.79	74.50

$m = 0.15$, $\alpha = 4.3^\circ$, axial feed = 0.37 mm/stroke.
[a]Per hammer.

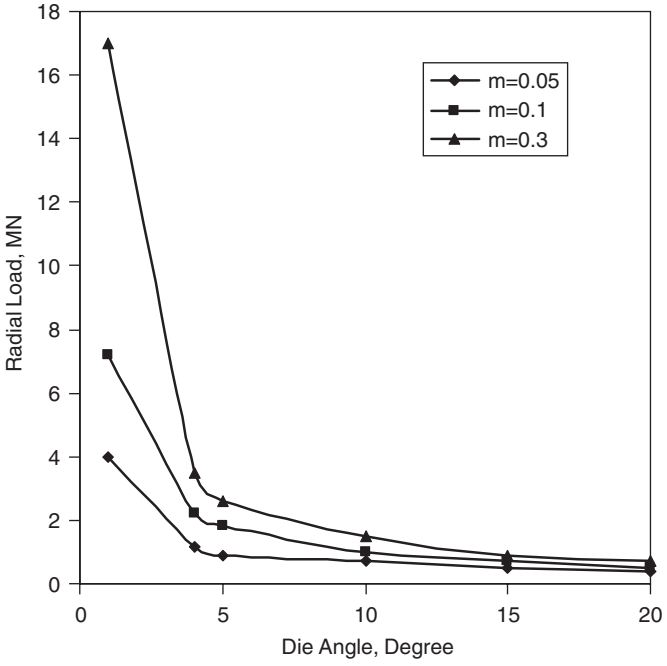

Fig. 8. The effect of die angle on the radial load per tool ($R_0 = 20$ mm, $R_1 = 16$ mm, $R_2 = 13$ mm, $R_m = 10$ mm, $m = 0.1$).

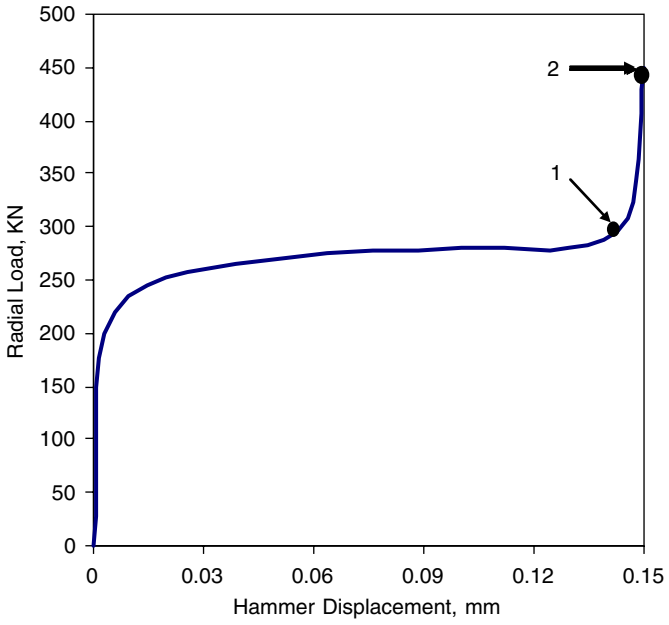

Fig. 9. The radial load per tool versus hammer displacement ($R_0 = 20$ mm, $R_1 = 16$ mm, $R_2 = 13$ mm, $R_m = 10$ mm, $m = 0.1$, $\alpha = 8^\circ$, axial feed = 1 mm/stroke).

where the length of forging zone and sizing zone are nearly equal. However, the predicted loads are higher when the forging zone is much smaller than the sizing zone which is the case in the finishing forging, see samples (3) and (4) in Table 1. According to Lahoti and Altan [7], this discrepancy may be attributed to the possibility of a lower friction in the sizing zone. It is interesting to note that the predicted load by the present approach is not so larger than predicted load by slab method during finish forging and it is even smaller in sample (4).

To verify the potential of the model for predicting the effects of process parameters, a further theoretical analysis was performed assuming that the material was AISI 1015 and the length of the sizing zone was equal to 18 mm. The results of this analysis are presented in various Figs. 8–11.

The effect of variation of die angle on the maximum radial load is plotted in Fig. 8. This figure reveals as the die angle increases, the radial load decreases because within a constant reduction in area, the length of contact and thus the frictional work decreases. Moreover, when the die angle increases, the radial component of die normal force reduces and the axial component increases. Therefore, one may conclude that there is a limitation to increasing the die angle, because if the die angle increases excessively, the axial load becomes so large that it may make the preform to either buckle or throw the part away from the forging box. Thus as the axial force is known, one can easily determine whether the part will buckle or not. Also, it is possible to predict the magnitude of the least required back-push force that prevents slipping of the part away. This force can also be used to find the maximum die angle within a certain process condition such as the reduction in area, and the length of preform, etc.

Variation of the radial load during the radial movement of the hammer die, since the hammer die touches the tube until it reaches to the end of stroke, is plotted in Fig. 9. As

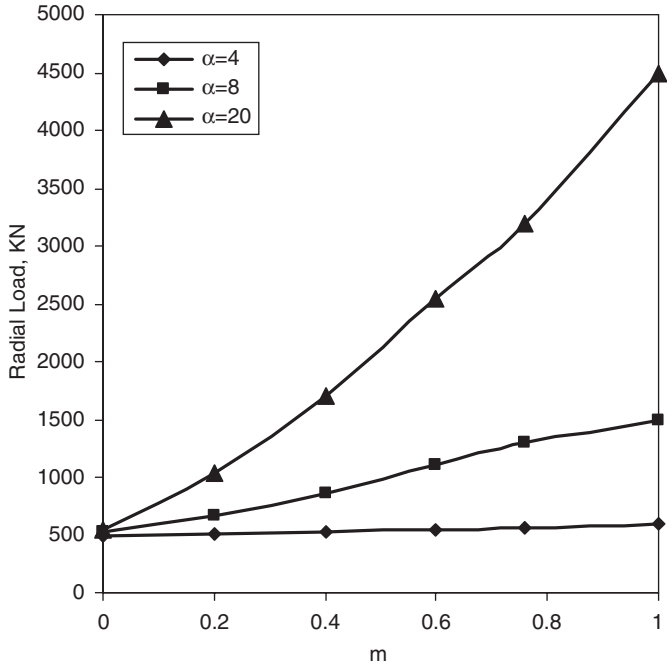

Fig. 10. The effect of m on the radial load per tool ($R_0 = 16$ mm, $R_1 = 12$ mm, $R_2 = 10$ mm, $R_m = 8$ mm, $\alpha = 4°$).

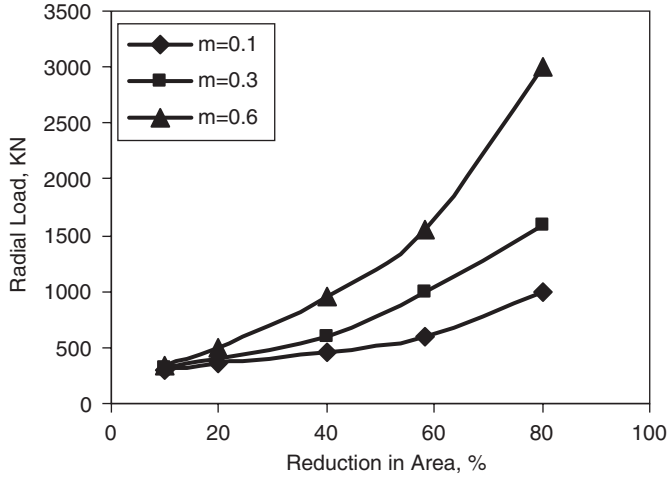

Fig. 11. The effect of reduction in area on the radial load per tool ($R_0 = 20$ mm, $R_1 = 16$ mm, $m = 0.1$, $\alpha = 8°$).

may be seen, after the hammer die touches the tube, the radial load gradually increases almost until the end of the stroke. At point marked (1) in Fig. 9, where the die land or sizing zone (III) touches the part, the radial load suddenly increases and then reaches its maximum value at the end of the stroke; see point (2) in Fig. 9.

Fig. 10 shows the effect of frictional shear factor m on the radial forging load at the end of the stroke. It is observed that when the frictional shear factor m increases, the radial load also increases due to the increase in frictional work.

Fig. 11 shows the effect of reduction in cross-sectional area of the tube on the radial load at the end of the stroke. In each case as it is observed, when the reduction is increased, the maximum required radial load also increases due to increase in all the work components, i.e. plastic, frictional and the shear work. It has been reported in reference [19] that in order to enjoy the benefits of the radial forging process, the reduction must be so large that the plastic deformation penetrates to the core of the material. Thus it is important to choose either a machine with enough capacity to forge the desired part in one pass or finding the minimum number of passes when it is not possible to forge the part in one pass. After calculating the maximum load, the maximum required rate of work can be obtained by multiplying the hammers speed by the maximum load. Obviously, if the calculated power is less than the machine power, the part can be produced in one pass. Otherwise, the part should be produced in more than one pass so that the power of each pass is less than the machine power.

4. Conclusions

In this research, a new approach based on calculating the work at various stages of the radial-forging process was presented to predict the maximum load required to deform the circular billet incrementally. For verification of the model, the load was predicted for cold forging of the rods, and then compared with those of the published experimental results of another author, see Ref. [1]. Also, the effect of various process parameters was assessed by the model and compared with the published results. A reasonably good agreement was found between the various sets of results.

Acknowledgments

The authors would like to acknowledge with gratitude for the financial support given to the project by the Research Board of Sharif University of Technology.

References

[1] Uhlig A, Investigation of the motions and the forces in radial swaging. Doctoral dissertation, Technical University Hannover, 1964.
[2] Altan T, Oh SI, Gegel H. Metal forming fundamentals and applications. Materials Park, OH: American Society for Metals; 1983. p. 17.
[3] GFM Precision Forging Machine, GFM Technical literature. October 1976.
[4] Tszeng TC, Kobayashi S. Determination of residual stresses in radial forging. Manufacturing Processes Simulation 1986;PED-20:31–45.
[5] Domblesky JP, Shivpuri R, Painter B. Application of finite-element method to the radial forging of large diameter tubes. Journal of Material Processing Technology 1995;49:57–74.
[6] Jang DY, Liou JH. Study of stress development in axi-symmetric products processed by radial forging using a 3-D finite-element method. Journal of Material Processing Technology 1998;74:74–82.

[7] Lahoti GD, Altan T. Analysis of the radial forging process for manufacturing of rods and tubes. Journal of Engineering for Industry 1976;98:265–71.
[8] Lahoti GD, Dembowski PV, Altan T. Radial forging of tubes and rods with compound-angle dies. In: Proceedings of NAMRC-IV, Columbus, OH. May 17–19 1976. p. 87–93.
[9] Subramanian TL, Venkateshwar R, Lahoti GD, Lee FM. Experimental and computer modeling of die cavity fill in radial forging of rifling. Process modeling—fundamentals and applications to metals. In: Proceedings of process modeling sessions, 1978 and 1979, USA.
[10] Yang S. Research into GFM forging machine. Journal of Material Processing Technology 1991;28:307–19.
[11] Thompson EG, Hamzeh O, Jackman LA, Srivatsa SK. A quasi-steady-state analysis for radial forging. Journal of Material Processing Technology 1992;34:1–8.
[14] Johnson W, Mellor PB. Engineering plasticity. Ellis Harwood Limited; 1983.
[15] Hosford WF, Caddell RM. Metal forming. Englewood Cliff, NJ: Prentice-Hall; 1993.
[16] Hung-Hsiou H. A study on precision forging of spur gear forms and splines by the upper bound method. International Journal of Mechanical Science 2002;44:1543–58.
[17] Chitkara NR, Aleem A. Extrusion of axi-symmetric bi-metallic tubes from solid circular billets: application of a generalized upper bound analysis and some experiments. International Journal of Mechanical Science 2001;43:2833–56.
[18] Bourkine SP, Babailov NA, Loginov YN, Shimov VV. Energy analysis of a through-put radial forging machine. Journal of Material Processing Technology 1999;86:291–9.
[19] Rauschnabel E, Schmidt V. Modern application of radial forging and swaging in automotive industry. Journal of Material Processing Technology 1992;35:371–83.
[12] Ameli A. Finite element simulation of the radial forging process. M.Sc. thesis, Sharif University of Technology, Tehran, 2004.
[13] Lahoti GD, Liuzzi L, Altan T. Design of dies for radial forging of rods and tubes. Journal of Mechanical Working Technology 1977;1(1):99.